KeA1

CHINESE ROOTS
GLOBAL IMPACT

Contents lists available at ScienceDirect

Petroleum Science

journal homepage: www.keaipublishing.com/en/journals/petroleum-science



Original Paper

Numerical investigation of refracturing with/without temporarily plugging diverters in tight reservoirs



Xiao-Hua Wang ^{a, b, c}, Feng-Shou Zhang ^{b, c, *}, Zi-Rui Yin ^{b, c}, Ding-Wei Weng ^d, Hong-Bo Liang ^d, Jun-Ping Zhou ^{e, f}, Bin Xu ^{g, h}

- ^a Shale Gas Research Institute, PetroChina Southwest Oil and Gas Field Company, Chengdu, 610051, Sichuan, China
- ^b Key Laboratory of Geotechnical & Underground Engineering of Ministry of Education, Tongji University, Shanghai, 200092, China
- ^c Department of Geotechnical Engineering, College of Civil Engineering, Tongji University, Shanghai, 200092, China
- d Research Institute of Petroleum Exploration and Development, PetroChina, Langfang, 065007, Hebei, China
- ^e State Key Laboratory of Coal Mine Disaster Dynamics and Control, Chongqing University, Chongqing, 400044, China
- f School of Resources and Safety Engineering, Chongqing University, Chongqing, 400044, China
- g Origin Geomechanics Inc., Calgary, T3H0X6, Canada
- ^h Department of Civil Engineering, University of Calgary, Calgary, T2N1N4, Canada

ARTICLE INFO

Article history: Received 27 January 2022 Received in revised form 6 May 2022 Accepted 8 May 2022 Available online 13 May 2022

Edited by Yan-Hua Sun

Keywords: Tight reservoir Hydraulic fracturing Temporary plugging Discrete lattice method Multi-cluster fracturing

ABSTRACT

Refracturing is an important technique to tap the potential of reservoirs and boost production in depleted oil and gas fields. However, fracture propagation during refracturing, including both conventional refracturing and temporary-plugging refracturing remains poorly understood, especially for cases with non-uniform distribution of formation pressure due to long-term oil production and water injection. Therefore, taking pilot tests of refracturing with sidetracking horizontal wells in tight reservoirs in the Changqing Oilfield, China as an example, we establish a three-dimensional numerical model of conventional refracturing and a numerical model of temporary-plugging refracturing based on the discrete lattice method. Non-uniform distributions of formation pressure are imported in these models. We discuss the effects of key operating parameters such as injection rate, cluster spacing, and number of clusters on the propagation of multi-cluster fractures for conventional refracturing. For temporaryplugging refracturing, we examine the impacts of controlling factors such as the timing and number of temporary plugging on fracture propagation. In addition, we analyze a field case of temporaryplugging refracturing using well P3 in the Changqing Oilfield. The results show that fractures during refracturing tend to propagate preferentially and dominantly in the depleted areas. Improved stimulation effect can be obtained with an optimal injection rate and a critical cluster spacing. The proposed model of temporary-plugging refracturing can well describe the temporary plugging of dominant existingfractures and the creation of new-fractures after fracturing fluid is forced to divert into other clusters from previous dominant clusters. Multiple temporary plugging can improve the balanced propagation of multi-cluster fractures and obtain the maximum fracture area. The established numerical model and research results provide theoretical guidance for the design and optimization of key operating parameters for refracturing, especially for temporary-plugging refracturing.

© 2022 The Authors. Publishing services by Elsevier B.V. on behalf of KeAi Communications Co. Ltd. This is an open access article under the CC BY-NC-ND license (http://creativecommons.org/licenses/by-nc-nd/4.0/).

1. Introduction

In the early development stage, a large number of vertical wells with hydraulic fracturing were used to develop tight oil reservoirs in the Changqing Oilfield, China. After long-term oil production and water injection, the production of the original vertical wells started to decrease significantly, and refracturing with sidetracking horizontal wells (Fig. 1d) drilled from the original vertical wells is an

E-mail addresses: wangxh199206@163.com (X.-H. Wang), fengshou.zhang@tongji.edu.cn (F.-S. Zhang), zirui.yin@tongji.edu.cn (Z.-R. Yin), wendw69@petrochina.com.cn (D.-W. Weng), lianghb69@petrochina.com.cn (H.-B. Liang), zhoujp1982@sina.com (J.-P. Zhou), binxu@origingeomechanics.com (B. Xu).

^{*} Corresponding author.

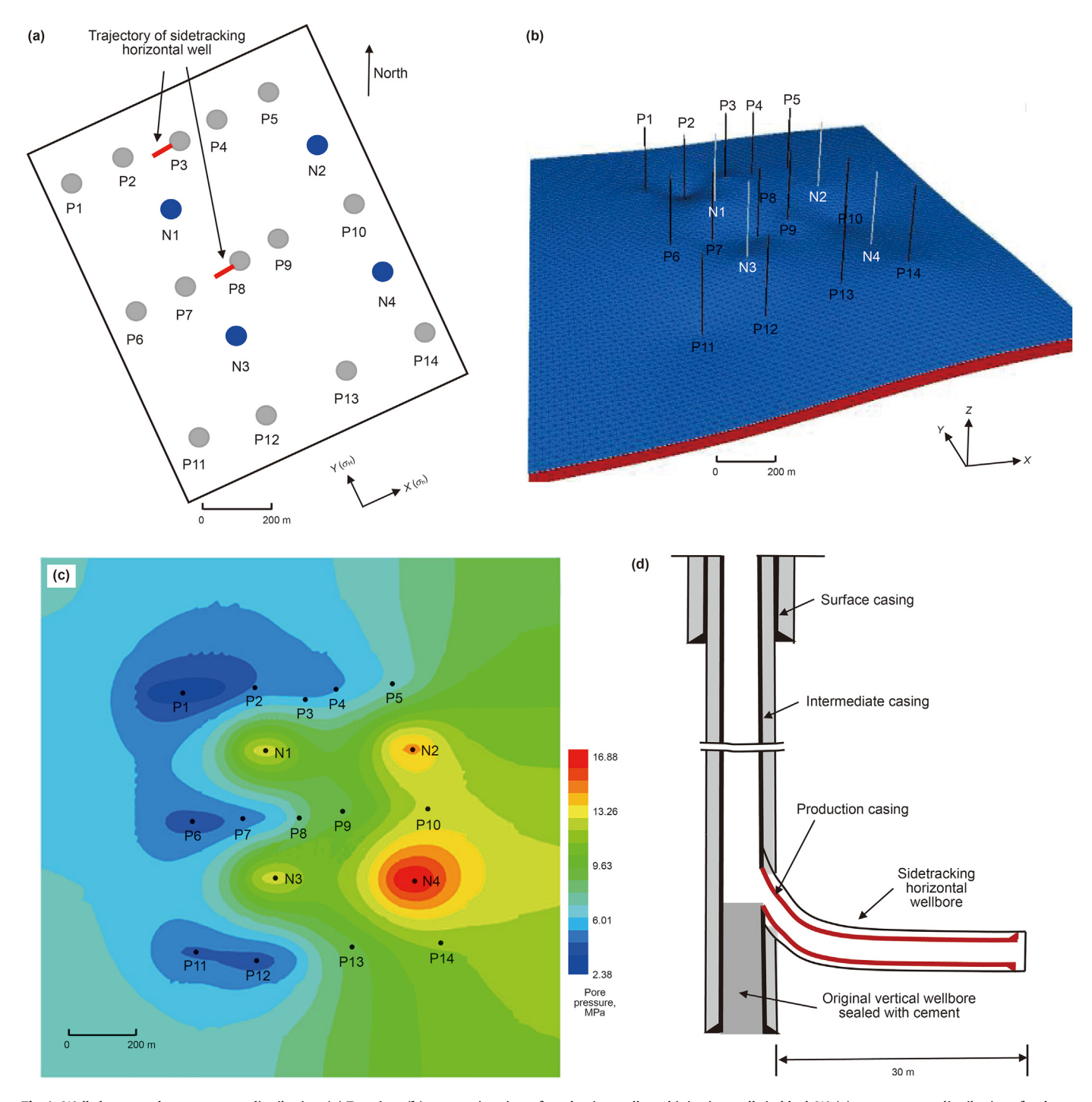


Fig. 1. Wells layout and pore pressure distribution. (a) Top view, (b) perspective view of production wells and injection wells in block W, (c) pore pressure distribution after long-term production and injection, and (d) sidetracking horizontal wells. The gray dots in Fig. 1(a) and the solid black lines in Fig. 1(b) represent the production wells, while the blue dots in Fig. 1(a) and the solid white lines in Fig. 1(b) represent the injection wells.

important measure to tap the potential and increase production. Refracturing with sidetracking horizontal wells is a completion technique that a horizontal wellbore aligned with the minimum horizontal stress direction in the target reservoir is firstly drilled from the original vertical wellbore (Wang et al., 2016; Yue et al., 2018; Zhang et al., 2019b), and then multi-cluster refracturing is carried out for the horizontal well (Roussel and Sharma, 2010; Wang and Salehi, 2014; Li et al., 2017; Shah et al., 2017; Ishida et al., 2019; Luo et al., 2020). Compared with the initial hydraulic

fracturing (Zhao et al., 2019; Tang et al., 2019; Tan et al., 2020, 2021; Xie et al., 2020; Li et al., 2020c; Mao et al., 2021), the distribution of formation pore pressure is spatially non-uniform before refracturing due to the long-term production and injection, resulting in the complex propagation behavior of hydraulic fractures during refracturing (Roussel and Sharma, 2012, 2013; Marongiu-Porcu et al., 2016; Sangnimnuan et al., 2018; Zhang et al., 2022). In addition, temporary plugging diverters, also called temporary agents, may be added during refracturing to temporarily block or

constrain the propagation of dominant fractures, thereby forcing fracturing fluid to divert into other fractures. This process is called temporary-plugging refracturing (Wang et al., 2019; Zhang et al., 2020a, 2021e; Chen et al., 2020; Shah et al., 2020), and the propagation behavior of hydraulic fractures during temporary-plugging refracturing is more complex than that during conventional refracturing. Therefore, it is of importance to conduct simulation and prediction of fracture propagation for refracturing, including conventional refracturing and temporary-plugging refracturing.

Many valuable studies have been carried out on fracture propagation during refracturing. In refracturing experiments, scholars have qualitatively investigated the influence of horizontal stress difference, fluid injection volume, natural fractures, and temporary plugging agent amount on fracture morphologies during refracturing (Li et al., 2019; Guo et al., 2020; Wang et al., 2020; Zhang et al., 2020b). In numerical simulation, Ren et al. (2010) established a mathematical model of induced stress field for refractured wells, and obtained fracture propagation path. Huang et al. (2016) showed that fractures with larger width and smaller length are produced by refracturing the pre-existing perforations. Rezaei et al. (2018) proposed a two-dimensional fully-coupled poroelastic displacement discontinuity method to simulate the entire propagation process of child fractures between two parent fractures in the depletion area. It was found that effective refracturing can be achieved within a specific time frame. Wang et al. (2018) and Li et al. (2020a) established numerical models of temporaryplugging staged fracturing using pore-pressure cohesive model and studied the impacts of stress contrast, formation permeability. tensile strength. Young's modulus, injection rate, cluster spacing. and number of clusters on fracture propagation. They found that with increasing stress difference, rock permeability, and Young's modulus, the diverting fracture deviates rapidly from the initial fracture direction. High injection rate improves the fracturing effect for temporary-plugging refracturing. However, these twodimensional models do not consider the propagation of the fracture height. Zou et al. (2020) used the plugged fracture elements with negligible permeability to characterize temporary plugging agent in fractures based on the three-dimensional finite discrete element method. They simulated the fracture propagation in fractured formations and recorded in detail the changes in injection pressure before and after temporary plugging under different conditions. However, the fracture height in their study is constant, and the distribution of formation pressure is not considered. Guo et al. (2019) established a refracturing productivity model, considering stress sensitivity under different production times, and optimized the temporary plugging number and the amount of temporary plugging agents. Zhang and Mack (2017) studied the effect of isolation and near-wellbore friction on the refracturing of an Eagle Ford well, using fully coupled geomechanical simulation and microseismic analysis. However, it is assumed that there is an even pressure drop of 10 MPa in the depletion zone, which does not consider the non-uniform distribution of formation pressure under realistic conditions. Yi and Sharma (2016) proposed a refracturing model for horizontal wells with temporary plugging diverters based on the PKN model and a flow resistance model. Diverter placement and multiple fracture propagation are quantitatively simulated. Yi and Sharma (2018) and Yi et al. (2019) calculated the distribution of fluid and proppants with multiple-cluster fractures during temporary-plugging refracturing. The distribution of fracturing fluid is non-uniform, and the fractures in twenty clusters receive the most fracturing fluid at the heel end. They suggest that using smaller length of refracturing section, and more frequent use of temporary plugging diverters can prevent excessive propagation of dominant fractures and promote uniform extension of multicluster fractures.

The aforementioned research revealed the fracture propagation during refracturing. However, heterogeneous formation pressure caused by long-term production and injection is rarely considered in the current refracturing studies. Therefore, further research is urgently needed to clarify the fracture propagation behavior under the impact of non-uniform formation pressure. In addition, it is rare to find three-dimensional numerical models of temporary-plugging refracturing considering the application of temporary plugging diverters that simulate the plugging of dominant fractures and the generation of new fractures. Consequently, the influences of key operational parameters of temporary-plugging refracturing, especially the effect of the timing and number of temporary plugging, on the balanced propagation of multiple fractures and the stimulation effect of refracturing remain unclear.

To this end, we take the pilot refracturing test of sidetracking horizontal wells in tight reservoirs in the Changqing Oilfield, China as an example, and establish a three-dimensional fully-coupled numerical model of conventional refracturing and a numerical model of temporary-plugging refracturing combined with the discrete lattice method. The spatially non-uniform distribution of formation pressure caused by long-term oil production and water injection from several vertical wells in the block W are implemented in these refracturing numerical models. For conventional refracturing, we study the effects of control parameters including injection rate, cluster spacing, and the number of clusters on the fracturing effect. For temporary-plugging refracturing, we explore the effects of key operating parameters such as the number and timing of temporary plugging on the fracture propagation.

2. Engineering background

The block W is located in the Ordos Basin, China, and the target reservoir is the Chang-6 tight reservoir. The average thickness of the Chang-6 tight reservoir is 10 m. The porosity and the permeability of the target reservoir are 13% and 0.23 mD, respectively. The geological parameters of the Chang-6 tight reservoir, the upper mudstone barrier, and the lower mudstone barrier are listed in Table 1. Thereinto, the *in-situ* stresses of the tight reservoir and the barrier layer including the overburden stress, the maximum and the minimum horizontal stresses, are obtained by the logging data such as the density, acoustic and neutron logging (Zhao et al., 2018). The fracture toughness and the porosity are empirical values gained by field engineers. On the basis of Darcy's law, the permeability of reservoir rock is measured by the gas permeability tester. In the early stage, vertical producing wells and water injection wells are placed in block W. There are eighteen vertical wells in the study area, including fourteen production wells and four water injection wells (Fig. 1a and b). The oil production well rows and water injection well rows are mainly aligned with the direction of the minimum horizontal stress. After decades of production, the productivity of the vertical wells has declined sharply, with an average

Table 1Physical properties of the tight reservoir and the barrier layer.

Physical properties	Tight reservoir	Barrier layer
$\sigma_{\rm v}/\sigma_{\rm H}/\sigma_{\rm h}$, MPa	33.37/28.36/25.69	37.11/31.54/28.57
Elastic modulus, GPa	11.5	26.7
Poisson's ratio	0.19	0.18
Tensile strength, MPa	3.34	4.80
Compression strength, MPa	64.24	120.42
Fracture toughness, MPa m ^{0.5}	3	5
Porosity, %	13	2
Permeability, mD	0.23	0.03

Note: σ_v is the vertical stress; σ_H and σ_h are the maximum and minimum horizontal principal stresses, respectively.

oil production rate of $0.1 \text{ m}^3/\text{day}$ per well, much lower than the initial production rate of $3.9 \text{ m}^3/\text{day}$.

Therefore, refracturing with sidetracking horizontal well shown in Fig. 1d is proposed to stimulate undeveloped areas. In the Chang-6 reservoir, a horizontal open-hole wellbore with a length of 30 m and a diameter of 118 mm along the minimum horizontal stress direction is drilled (the red bold lines in Fig. 1a). Then, spiral perforation with a phase angle of 60° is carried out by a hydraulic jet in the horizontal wellbore. There are three clusters with a cluster spacing of 10 m. Each cluster has six perforation tunnels with a diameter of 20 mm and a length of 1 m. Fracturing fluid is injected at a rate of 3 m $^3/$ min and with fluid viscosity of 100 mPa s.

To date, pilot tests of refracturing with sidetracking horizontal wells have been carried out in well P8 and well P3. Specifically, conventional refracturing without temporary plugging diverters is used for well P8, and temporary-plugging refracturing with temporary plugging diverters for well P3. The spatial non-uniform distribution of the formation pressure in block W before refracturing is calculated (Fig. 1c) by using the finite difference code FLAC3D. It is clear from Fig. 1c that the pore pressure around the injection wells is usually higher, while it is lower around the production wells. Furthermore, the heterogeneous formation pressures in the vicinity of well P8 and well P3 before refracturing (shown in Figs. 2b and 9b) can be extracted from Fig. 1c, respectively. The distribution of formation pressure is very complex, with a maximum variation of 4 MPa, which significantly affects the propagation behavior of hydraulic fractures during refracturing.

Therefore, fracture propagation of conventional refracturing for well P8 and fracture propagation of temporary-plugging refracturing for well P3 are investigated in this work to provide theoretical guidance for the design and optimization of refracturing operation parameters.

3. Discrete lattice method

The simulation of initiation and propagation of hydraulic fractures using the discrete lattice method has been widely used in petroleum industry (Bakhshi et al., 2019, 2021; Zhang et al., 2019a, 2021b; Nadimi et al., 2020; Huang et al., 2020; Wu et al., 2021; Wang et al., 2022a, b).

(1) The lattice

The lattice used in the discrete lattice method is a quasi-random assembly of nodes connected by nonlinear springs. The discrete lattice method uses an explicit solution scheme, which is suitable for direct simulation of highly nonlinear behavior. The motion law of translational degrees of freedom consists of the following central difference formulas for each node (Damjanac et al., 2011, 2016),

$$\begin{cases} \dot{u}_{i}^{(t+\Delta t/2)} = \dot{u}_{i}^{(t-\Delta t/2)} + \sum_{i} F_{i}^{(t)} \Delta t / m \\ u_{i}^{(t+\Delta t)} = u_{i}^{(t)} + \dot{u}_{i}^{(t+\Delta t/2)} \Delta t \end{cases}$$
(1)

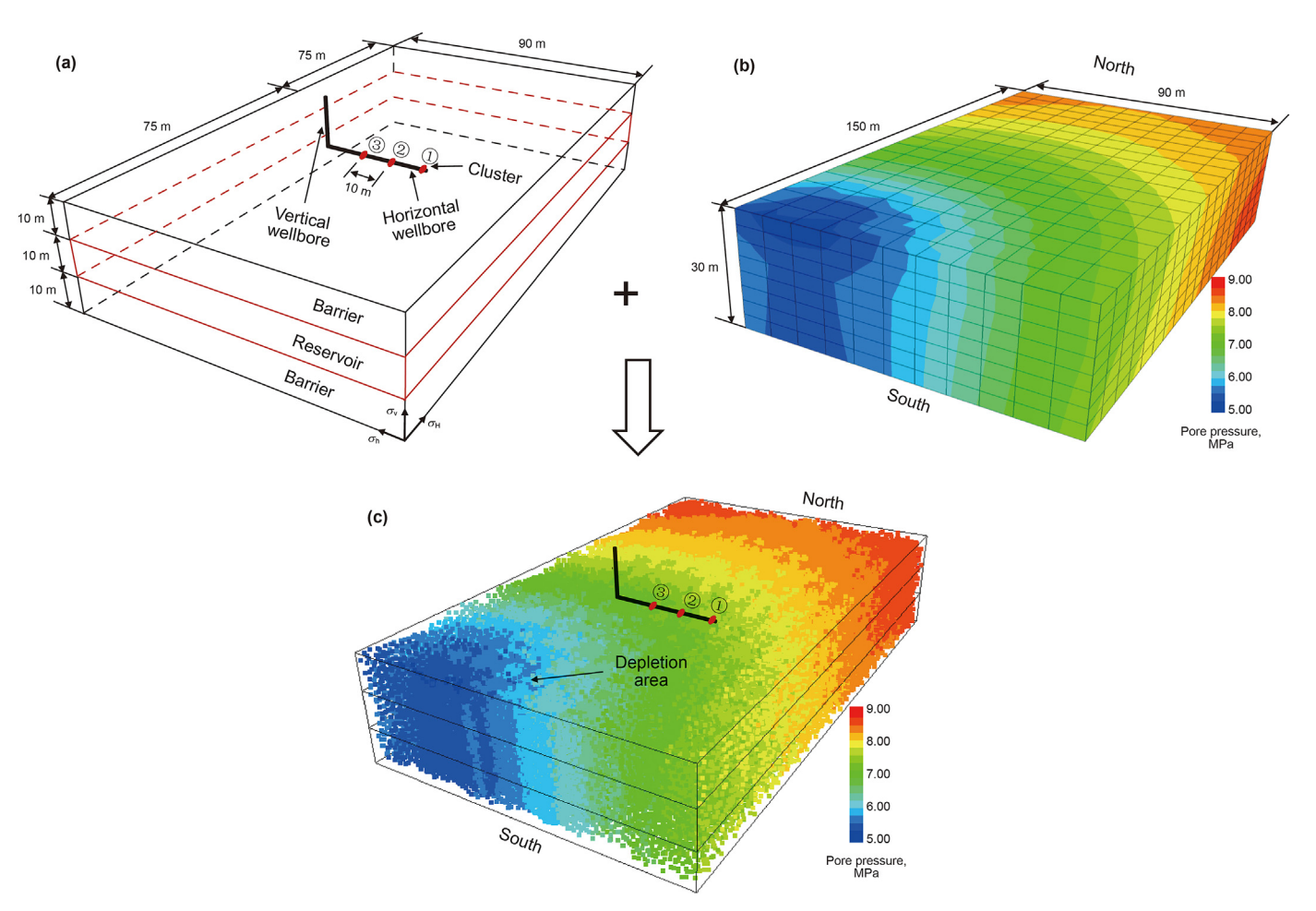


Fig. 2. (c) A three-dimensional refracturing numerical model is obtained by importing (b) the non-uniform formation pressure into (a) the fracturing numerical model.

where $u_i^{(t)}$ and $u_i^{(t)}$ are the velocity and position of component i (i = 1, 3), respectively, $\sum F_i$ is the sum of all force components i (i = 1, 3) acting on the node with mass m, and Δt is the time step.

The angular velocity w_i of component i (i = 1, 3) is calculated by the central difference equation as (Damjanac et al., 2011, 2016),

$$w_i^{(t+\Delta t/2)} = w_i^{(t-\Delta t/2)} + \frac{\sum M_i^{(t)}}{I} \Delta t$$
 (2)

where $\sum M_i$ is the sum of all moment component i (i = 1, 3).

The normal force F^N and tangential force F^S of the spring are calculated by (Damjanac et al., 2011, 2016),

$$\begin{cases} F_i^N \leftarrow F_i^N + \dot{u}_i^N K^N \Delta t \\ F_i^S \leftarrow F_i^S + \dot{u}_i^S K^S \Delta t \end{cases}$$
 (3)

where K^N is the normal stiffness, and K^S is the tangential stiffness. Finally, a new spring force is added to the force sum of the associated nodes (Damjanac et al., 2011, 2016) as

$$\begin{cases} \sum F_i^{A} \leftarrow \sum F_i^{A} - F^{N} n_i - F_i^{S} \\ \sum F_i^{B} \leftarrow \sum F_i^{B} + F^{N} n_i + F_i^{S} \end{cases}$$

$$(4)$$

where vector n_i is the unit normal vector from node A to node B.

Note that the normal force of the spring is positive in tension. After Eq. (3) calculation, the normal force test of the breakage is carried out. When $F^{\rm N} > F^{\rm Nmax}$ or $F^{\rm S} > F^{\rm Smax}$, the spring will break in tension or shear, respectively. After the spring breaks, microcracks are generated, and the spring force is reset to zero. At this time, $F^{\rm N} = 0$, $F^{\rm S} = 0$.

(2) Flow model

It is assumed that the width of the pipe in the joint plane is equal to its length. The flow rate from fluid node A to node B along the pipeline is calculated as (Damjanac et al., 2011, 2016),

$$q = \beta k_{\rm r} \frac{a^3}{12\mu} \Big[p^{\rm A} - p^{\rm B} + \rho_{\rm w} g \Big(z^{\rm A} - z^{\rm B} \Big) \Big]$$
 (5)

where β is the calibration factor, $k_{\rm r}$ is the relative permeability, a is the fracture width, μ is the fluid viscosity, $p^{\rm A}$ and $p^{\rm B}$ are fluid pressures at nodes A and B, respectively, $\rho_{\rm w}$ is the fluid density, g is the acceleration of gravity, and $z^{\rm A}$ and $z^{\rm B}$ are the heads at nodes A and B, respectively.

The evolution of the fluid model over time is solved by an explicit numerical scheme. The fluid pressure increases Δp for the time step $\Delta t_{\rm f}$ is (Damjanac et al., 2011, 2016)

$$\Delta p = \frac{\sum q_i}{V} \overline{K}_F \Delta t_f \tag{6}$$

where q_i is the injection rate of the pipe connected to node i, \overline{K}_F is the apparent fluid bulk modulus, and V is the node volume.

Generally, the migration of fluid in porous media involves the interaction between fluid and solid (Zhang et al., 2020c, 2021c,d; Cong et al., 2022), and thereby the mechanical and fluid models in the discrete lattice method are fully coupled to simulate hydraulic fracturing (Damjanac et al., 2011, 2016). Fracture permeability and fluid pressure affect the deformation of the mechanical model, while the deformation of the mechanical model in turn affects the fracture permeability and fluid pressure. It is noted that we do not consider the temperature impact on the fracture propagation and

the performance of temporarily plugging diverters in this work, in that our study focuses on the conventional oil and gas reservoirs rather than the enhanced geothermal systems.

4. Fracture propagation of conventional refracturing

The pilot test of conventional refracturing without temporary plugging diverters was conducted in well P8 of block W, which is mainly used to evaluate the effect of conventional operational parameters on multi-cluster fracturing.

4.1. Numerical schemes and numerical model

The numerical schemes of conventional refracturing are given in Table 2. The influences of injection rate, cluster spacing, and the number of clusters on the initiation and non-uniform propagation of multi-cluster fractures during refracturing are mainly evaluated.

The non-uniform evolution of formation pressure near well P8 due to the long-term production and injection of eighteen wells in block W is shown in Fig. 2b, which is extracted from Fig. 1c. We find that the magnitude of formation pressure decreases gradually from the northeast to the southwest of the numerical model, and there is a large depletion area in the southwest corner. Fig. 2a shows the fracturing numerical model based on the discrete lattice method with a size of 150 m \times 90 m \times 30 m. The thicknesses of the tight reservoir, the upper barrier, and the lower barrier are all 10 m. The sidetracking horizontal wellbore with a length of 30 m is oriented along the direction of the minimum horizontal stress. Three clusters are arranged on the horizontal wellbore. The first cluster is placed at the toe of the horizontal wellbore, with a cluster spacing of 10 m. The refracturing model shown in Fig. 2c is obtained by importing the non-uniform formation pressure (Fig. 2b) into the fracturing model (Fig. 2a). The geological conditions and operational parameters in the numerical model are listed in Table 1 and section 2, respectively. Our study mainly focuses on the propagation of multiple fractures in the field scale, and thus an initial discshaped fracture perpendicular to the horizontal wellbore is assumed for each cluster instead of the realistic perforation tunnels. And then a sphere with the same radius as the disc-shaped fracture is set at the center of each disk-shaped fracture, which is the injection point of fracturing fluid. In addition, our model has about 1.0 million nodes, and it took about one day to run for each refracturing case, if using a computational station with Intel® Xeon® Processor E5-2690 v4, 128G memory. It is noted that the initial in-situ stresses in our model are constant and applied by stress boundary conditions. On the one hand, this is to simplify and reduce the interference of other factors; on the other hand, it is difficult to consider the non-uniform in-situ stresses in the discrete lattice method. Besides, an intact wellbore is assumed, and thus lost circulation (Feng et al., 2016) and interface debonding (Feng et al., 2017) are not considered in our model.

Table 2Numerical schemes of conventional refracturing.

Numerical scheme	Number of clusters	Cluster spacing, m	Injection rate, m ³ / min	
C1	3	10	3	
C2	3	10	2	
C3	3	10	4	
C4	2	10	3	
C5	4	10	3	
C6	3	8	3	
C7	3	12	3	

4.2. Typical numerical results of conventional refracturing

The effective clusters and the normalized standard deviation of fracture area are introduced to quantitatively describe the influence of different factors on the stimulation effect of refracturing. Based on previous evaluations of effective clusters (Mientka et al., 2018; Zhang et al., 2021a) and actual field conditions, a cluster is considered effective when its fracture area is greater than 80% of the average area, as shown in Eq. (7). The normalized standard deviation shown in Eq. (9) of the normalized fracture area (Eq. (8)) is used to describe the propagation uniformity of multi-cluster fractures as

$$A^{i} \ge \frac{\sum_{j=1}^{N} A^{i}}{N} \times 80\% \tag{7}$$

where A^i is the fracture area of the i-th cluster, and N is the number of clusters.

$$\xi^i = \frac{A^i}{\sum_{i=1}^N A^i} \tag{8}$$

$$S = \sqrt{\frac{\sum_{j=1}^{N} \left(\xi^{i} - \overline{\xi}\right)^{2}}{N}}$$
 (9)

where ξ^i is the normalized fracture area, $\overline{\xi}$ is the average normalized fracture area, and S is the normalized standard deviation.

The typical simulation results of conventional refracturing with an injection rate of 2 m³/min are displayed in Figs. 3–5. Only one planar fracture is effectively formed in the third cluster, which propagates asymmetrically in the north wing and the south wing. Similarly, the in-situ stress disturbance after refracturing is also just limited to the vicinity of the fracture in the third cluster which is shown in Fig. 4. The length of the north wing of this fracture is 36.0 m, significantly shorter than the south wing of 50.3 m. The reason is that the formation pressure in the north region is significantly higher than that in the south region. The breakdown pressure is 53.91 MPa, as shown in Fig. 3a. Although there is only one planar fracture propagating during refracturing, the extension pressure fluctuates greatly with a maximum variation of 4.50 MPa

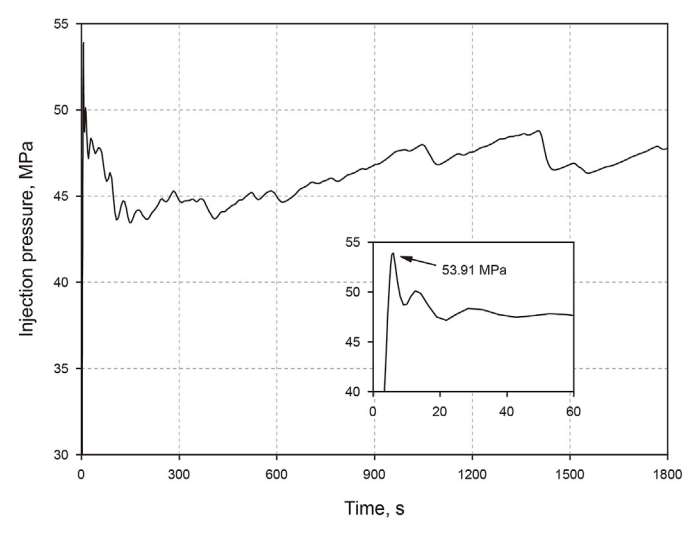
due to uneven distribution of the formation pressure, which is different from the characteristics of stable extension pressure when a single fracture propagates in a homogeneous layer (Zhu et al., 2015; Li et al., 2020b). As can be seen from Fig. 3b, fractures are initiated from all three clusters in the early stage (0–62.7 s). After that, the fractures in the first and second clusters cease propagating, and only the fracture in the third cluster continues to propagate effectively. In addition, the fracture area of the third cluster increases rapidly in the early stage, and the increment of fracture area decreases gradually later, indicating that the long-term injection of fracturing fluid has limited contribution to the improvement of stimulation.

4.3. Influence of operational parameters on conventional refracturing

4.3.1. Injection rate

Fig. 5 shows the fracture morphologies of refracturing with different injection rates. It can be seen that the fracture in the third cluster near the depletion area with different injection rates is dominant, which indicates that refracturing fractures tend to propagate preferentially and predominantly in the depletion area. Since the depletion area is usually the stimulated area after initial hydraulic fracturing, it is recommended to use a low-rate repressurization strategy or the shut-in before refracturing in order to increase the formation pressure in the depletion area, thereby reducing the propagation of refracturing fractures to the depletion area (Manchanda et al., 2017; Zhang and Mack, 2017).

In addition, as the injection rate is increased from 2 to 4 m³/min, the number of effective clusters is increased from 1 to 2, but no fractures are formed in the middle cluster (the second cluster) due to the stress shadow effect (Taghichian et al., 2014; Liu et al., 2018; Gutierrez Escobar et al., 2019). The normalized standard deviation of fracture area reduces with the increase of injection rate, by 42.50% and 13.04%, respectively (Fig. 6). With increasing injection rate, the total fracture area augments, but the increment amplitude is gradually reduced by 27.98% (964.07 m²) and 0.24% (10.51 m²), respectively. We find that high injection rate is helpful to improve the balanced propagation of multi-cluster fractures and achieve better fracturing effects. However, the increase of fracturing effect is limited when the injection rate is too high, and the optimal injection rate in this case is 3 m³/min.



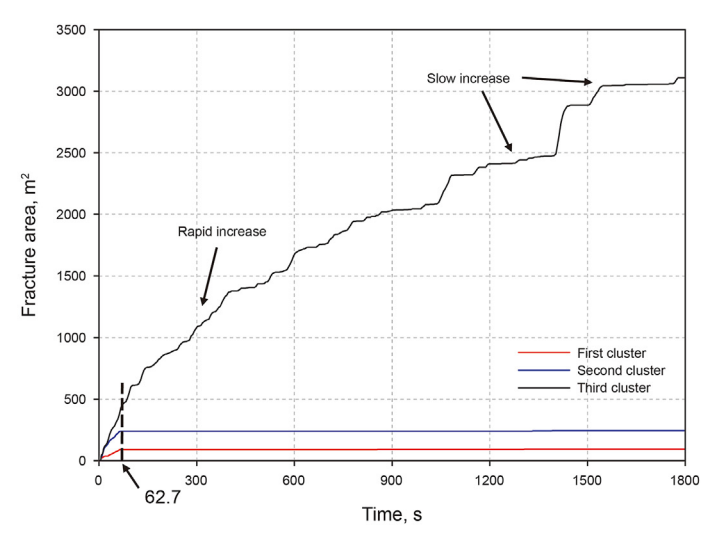


Fig. 3. Evolutions of (a) injection pressure, and (b) fracture area with an injection rate of 2 m³/min.

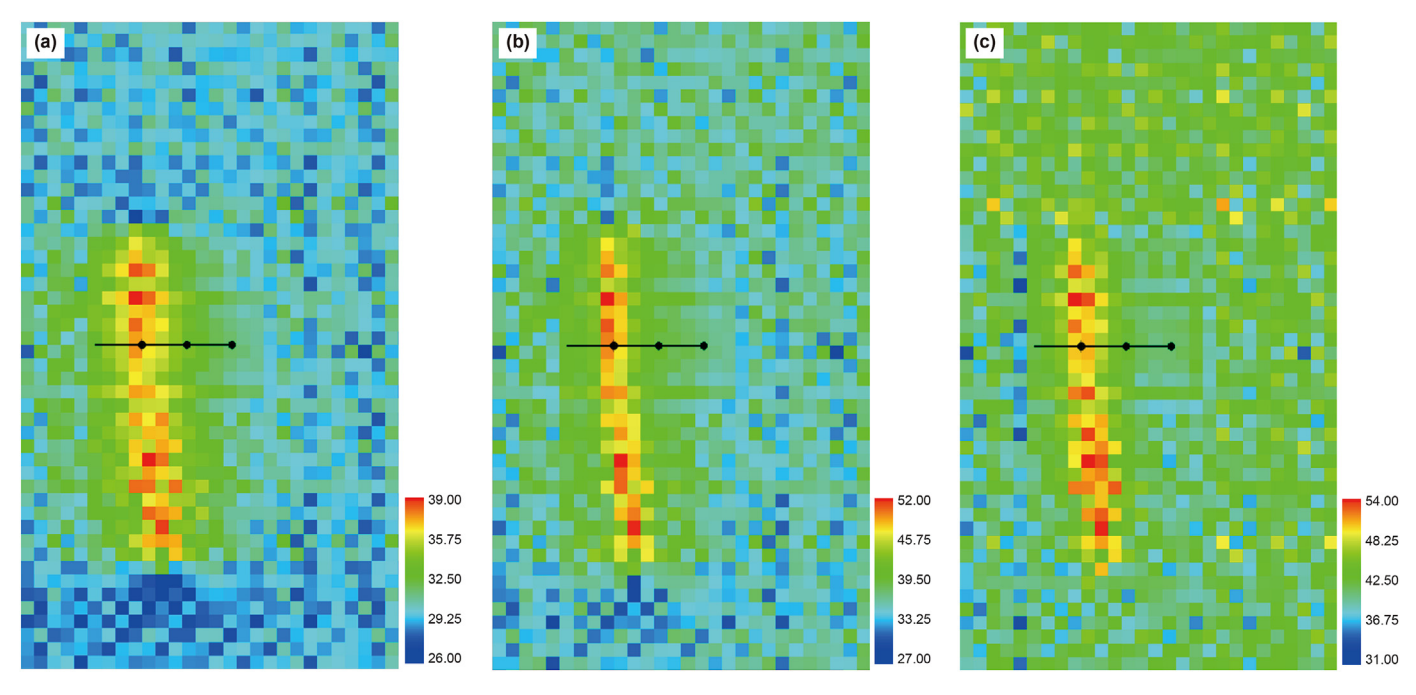


Fig. 4. Stress distributions after refracturing for the case with an injection rate of 2 m³/min. (a) The minimum principal stress, (b) the intermediate principal stress, and (c) the maximum principal stress.

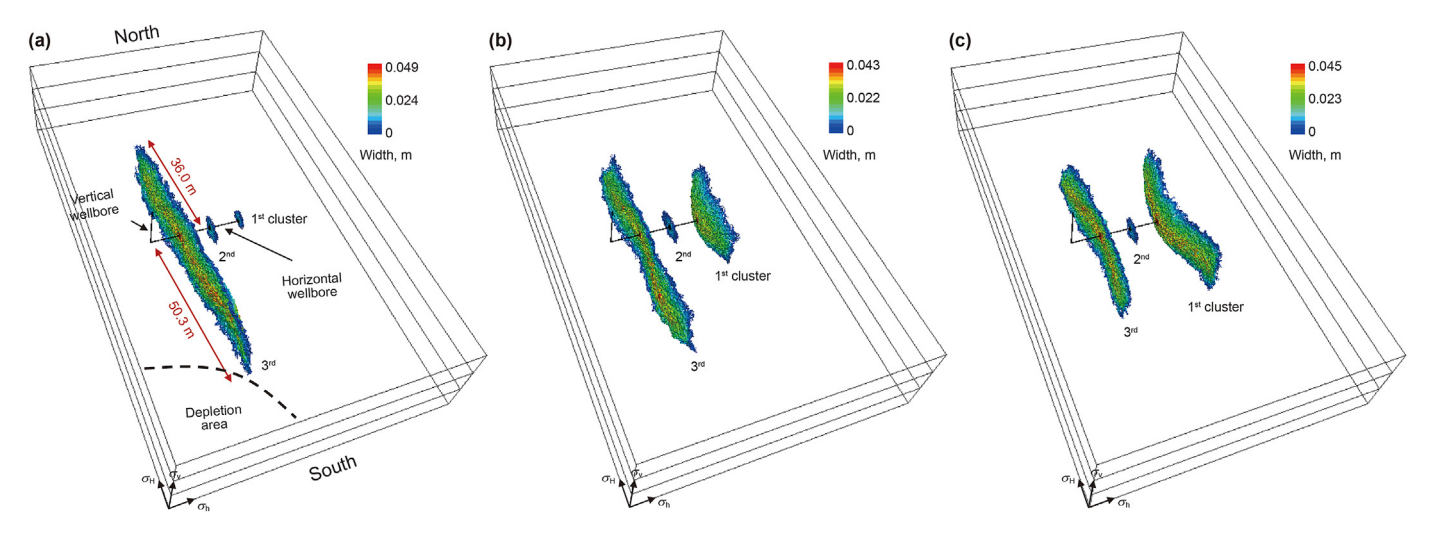


Fig. 5. Fracture morphologies of conventional refracturing with different injection rates of (a) 2 m³/min, (b) 3 m³/min, and (c) 4 m³/min.

4.3.2. Cluster spacing

Fig. 7 shows the fracture morphologies of refracturing under different cluster spacings. As the cluster spacing increases from 8 to 12 m, the fracture length of the third cluster, which is predominantly propagated, decreases gradually (Fig. 7), with a maximum reduction of 31.4 m. Results show that increasing cluster spacing can reduce the propagation of dominant fractures in the depletion area. With the increase in cluster spacing, the normalized standard deviation of the fracture area is reduced first and then increased (Fig. 6), indicating that the improvement of balanced propagation of multi-cluster fractures is limited when the cluster spacing exceeds the critical value of 10 m. With increasing cluster spacing, the total area of hydraulic fractures is increased by 1030.13 m² first, and then decreased by 560.34 m². The optimal cluster spacing is determined on the basis of the total fracture area and the balanced propagation of multi-cluster fractures (i.e., normalized standard

deviation). From Fig. 6b and c, when the cluster spacing is 10 m, the normalized standard deviation is the smallest, whereas the total fracture area is the largest. Therefore, the optimal cluster spacing is 10 m.

4.3.3. Number of clusters

Fracture morphologies of refracturing under different numbers of clusters are shown in Fig. 8. Only one fracture is generated from the second cluster near the wellbore for the case with two clusters, while two fractures are effectively formed for the case with three clusters. In the case of two clusters, because the spacing between adjacent clusters is only 10 m, the effect of stress shadow is large, inhibiting the fracture propagation from another cluster. In the case of three clusters, the spacing between the first cluster and the third cluster is 20 m, and the stress interference of the third fracture to the first fracture is relatively small, resulting in the effective

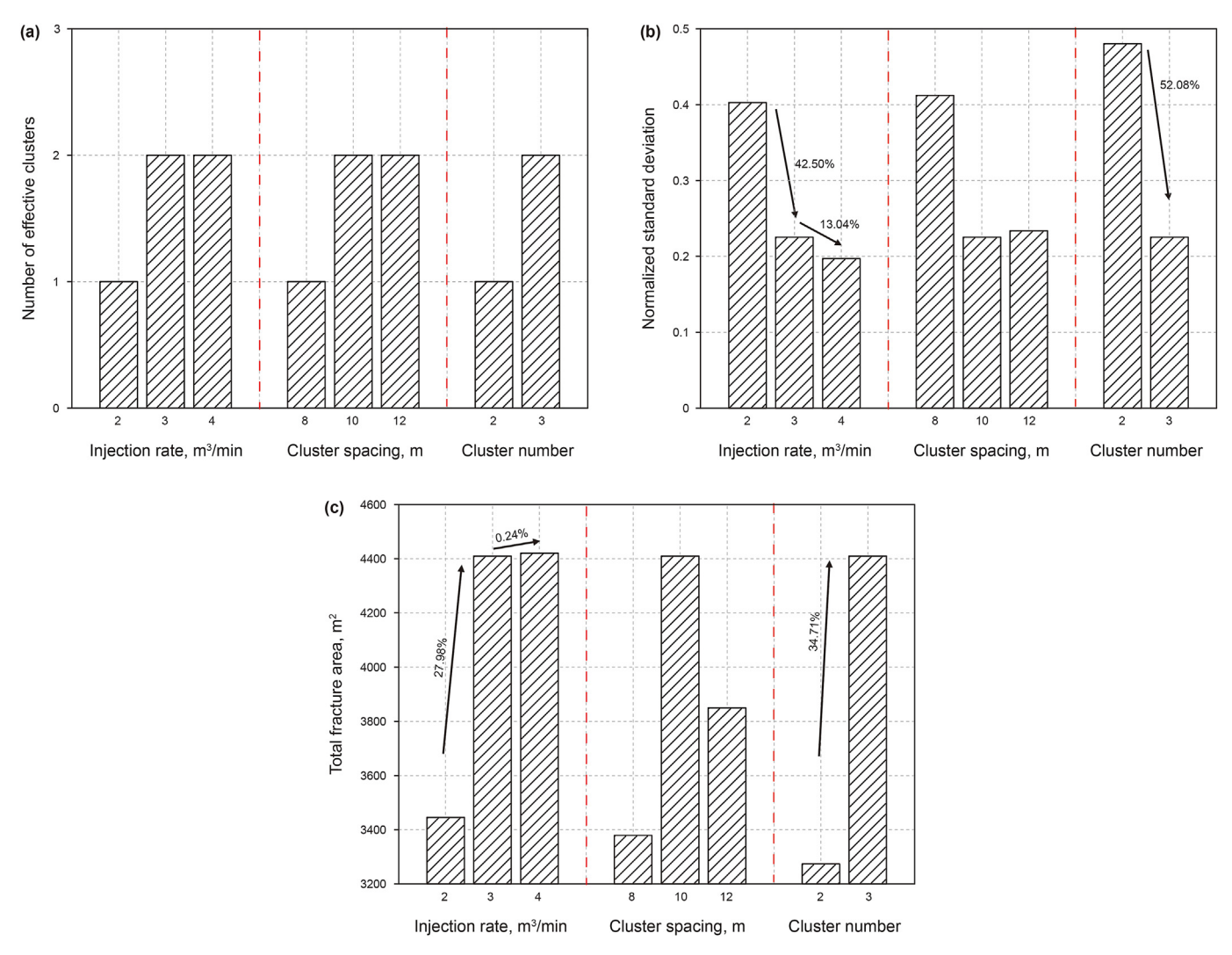


Fig. 6. Simulation results of (a) number of effective clusters, (b) normalized standard deviation, and (c) total fracture area under different operational parameters.

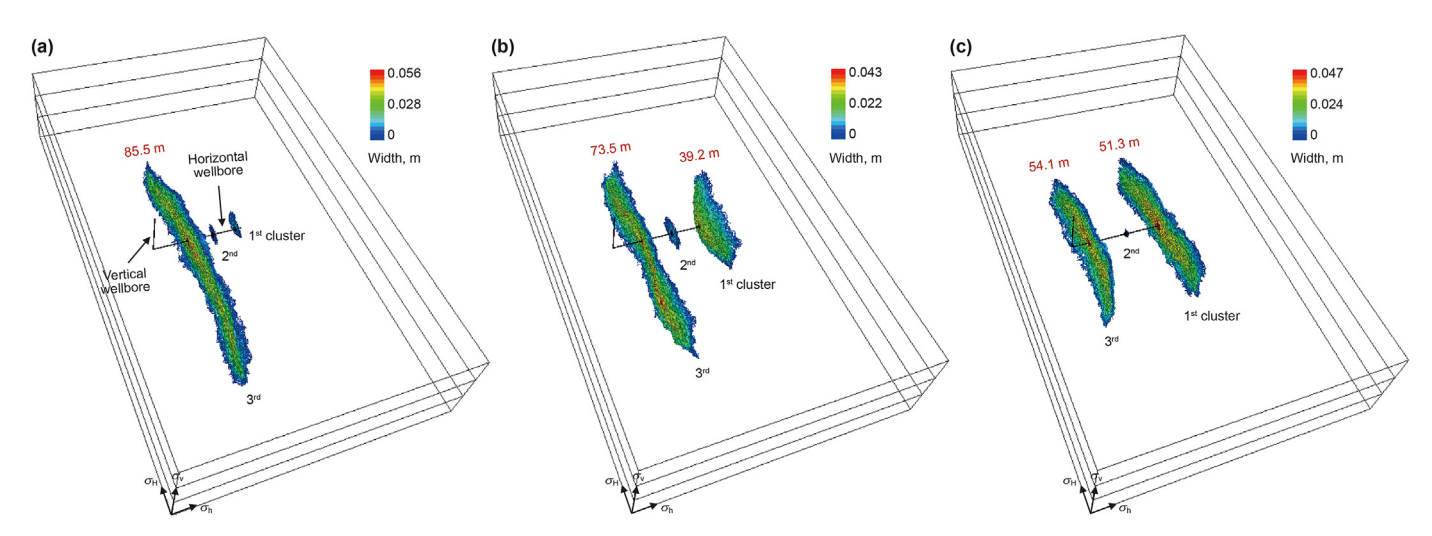


Fig. 7. Fracture morphologies of conventional refracturing with different cluster spacings of (a) 8 m, (b) 10 m, and (c) 12 m.

propagation of the first cluster. Therefore, in the case of two clusters, it is recommended to increase the cluster spacing appropriately to promote the effective propagation of fractures. In addition, as the number of clusters increases from 2 to 3, the total fracture

area is increased by 1136.27 m², an increase of 34.71%, while the normalized standard deviation of fracture area is reduced by 52.08%, indicating that the propagation uniformity of fractures increases greatly significantly.

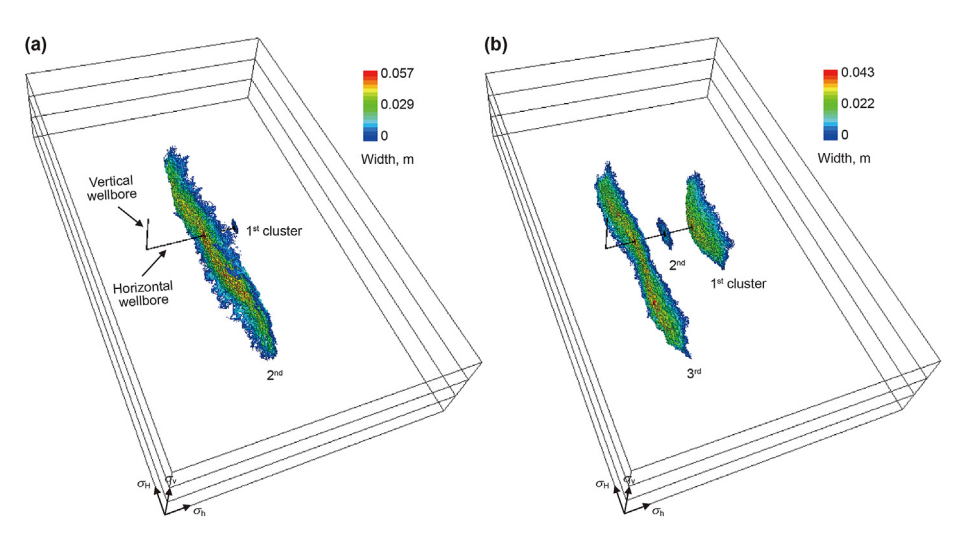


Fig. 8. Fracture morphologies of conventional refracturing with different numbers of clusters, (a) 2 clusters, and (b) 3 clusters.

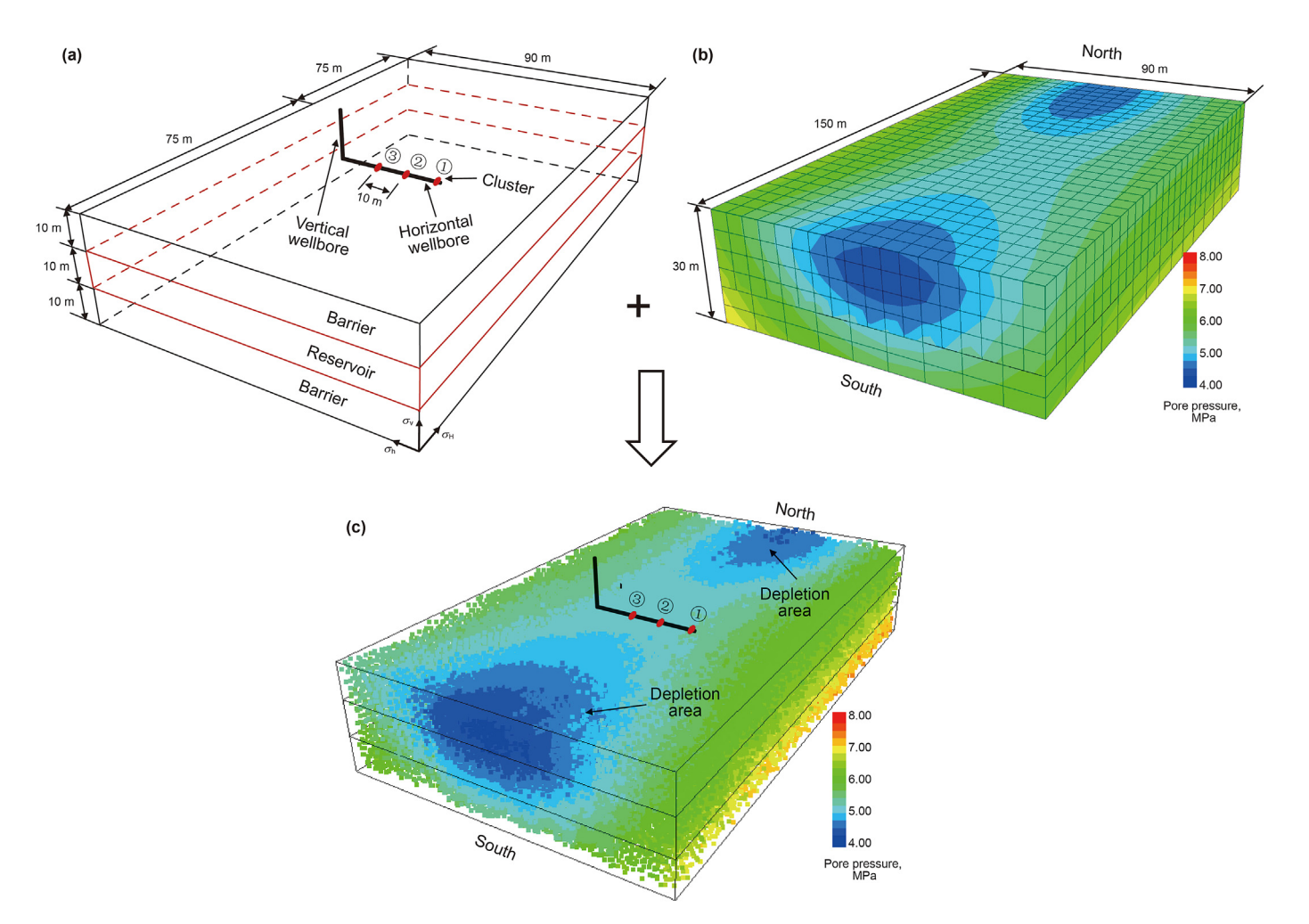


Fig. 9. (a) The non-uniform formation pressure near well P3 is imported into (b) the fracturing model to establish (c) the temporary-plugging refracturing model.

5. Fracture propagation of temporary-plugging refracturing

The pilot test of temporary-plugging refracturing with temporary plugging diverters for well P3 in block W is conducted to evaluate the influence of key parameters such as the timing and number of temporary plugging on the propagation of multi-cluster fractures.

5.1. Numerical schemes and model of temporary-plugging refracturing

The numerical schemes of temporary-plugging refracturing are provided in Table 3, and the impacts of the timing and number of temporary plugging are considered.

Table 3Numerical schemes of temporary-plugging refracturing.

Numerical scheme	Number of temporary plugging	Temporary plugging timing, s
1	0	_
2	1	300
3	1	400
4	1	500
5	1	600
6	1	700
7	1	800
8	1	900
9	2	300, 600
10	2	300, 700
11	2	300, 800
12	2	300, 900
13	2	400, 700
14	2	400, 800
15	2	400, 900
16	2	500, 800
17	2	500, 900
18	2	600, 900

The non-uniform formation pressure near well P3 after long-term production and injection (Fig. 9b) is extracted from Fig. 1c.

The numerical model of temporary-plugging refracturing shown in Fig. 9c is then built by importing the non-uniform formation pressure near well P3 (Fig. 9b) into the fracturing numerical model (Fig. 9a). All other settings of the temporary-plugging refracturing model are the same as those of the conventional refracturing model in Fig. 2a. The main difference between the two models is the difference in the formation pressure distribution and the use of temporary plugging diverter. The formation pressure near well P3 is relatively low on the north side and the south side of the numerical model, and there are depleted zones on both sides (Fig. 9). Importantly, in our numerical model of temporary-plugging refracturing, it is assumed that if a temporary plugging diverter is applied at a given time, the most dominant fracture is completely plugged and the propagation is stopped, and the injection pressure of this cluster remains constant. It is noted that in the discrete lattice method, the code simulates placement of the diverters. At any stage of simulation, the user can specify the number of diverters that are dropped into the wells. The same number of the perforation tunnels are plugged in the order from the one with the greatest flow rate to the one with the smallest flow rate. The perforation tunnels that are plugged do not take fluid anymore. The geological parameters and operational parameters of the model are shown in Table 1 and Section 2.

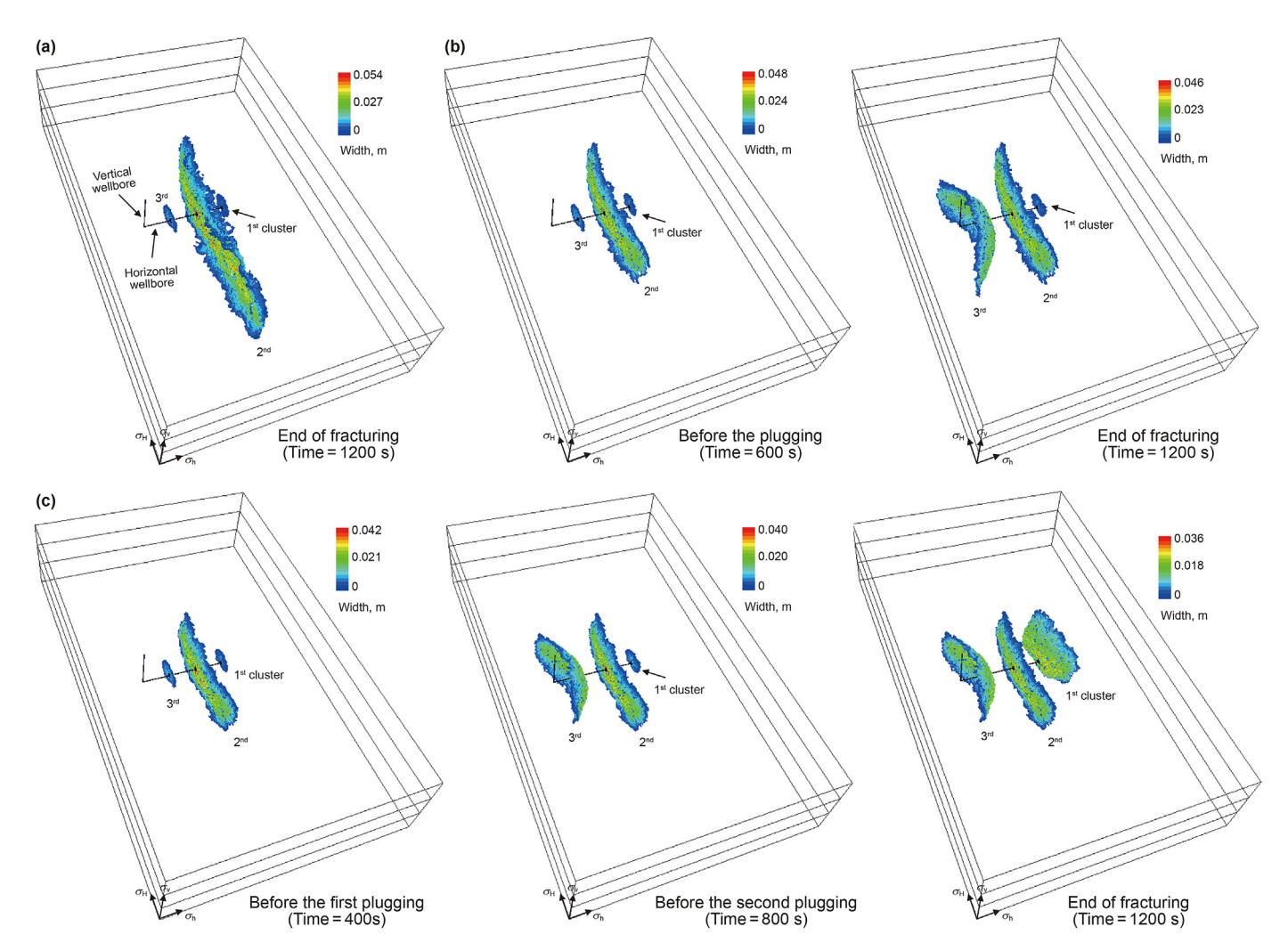


Fig. 10. Fracture morphologies of typical cases of temporary-plugging refracturing. (a) The number of temporary plugging is 0, (b) the number of temporary plugging is 1, with corresponding timing of 600 s, and (c) the number of temporary plugging is 2, with corresponding timing of 400 and 800 s, respectively.

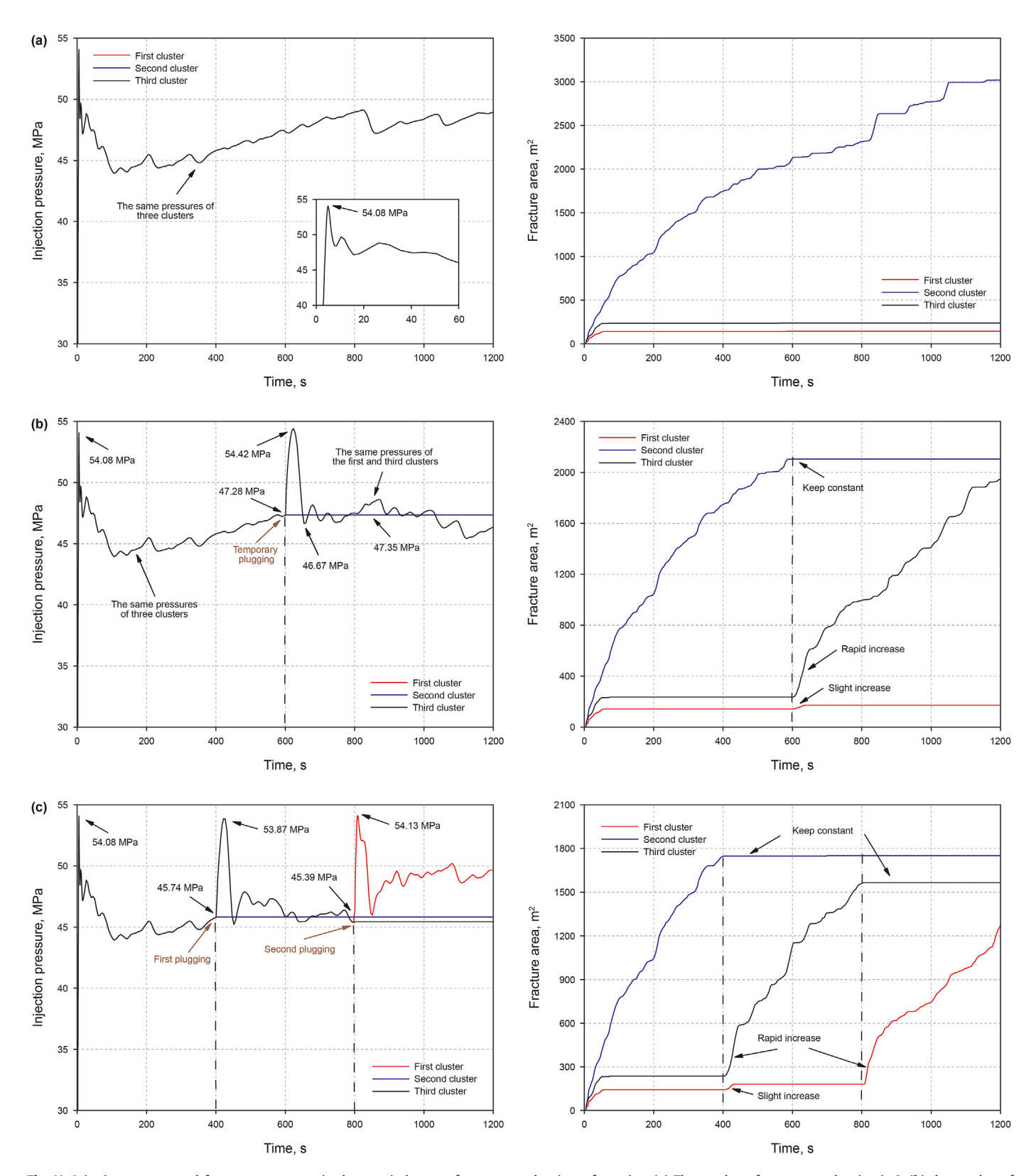


Fig. 11. Injection pressure and fracture area curves in three typical cases of temporary-plugging refracturing. (a) The number of temporary plugging is 0, (b) the number of temporary plugging is 1, with corresponding timing of 600 s, and (c) the number of temporary plugging is 2, with corresponding timing of 400 and 800 s, respectively.

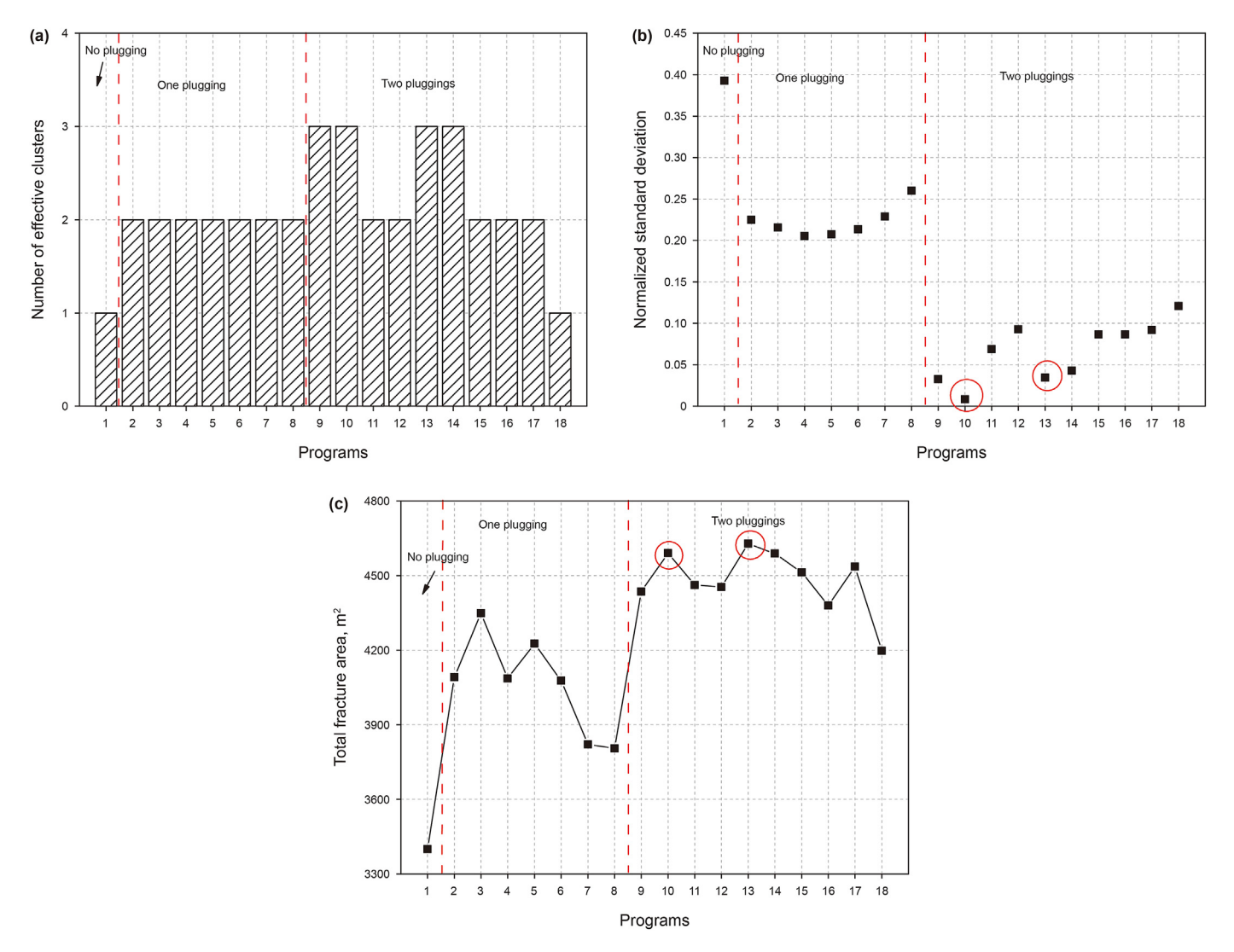


Fig. 12. (a) The number of effective clusters, (b) normalized standard deviation of fracture area, and (c) total fracture area under different numbers of temporary plugging. Red circles mark the corresponding optimal schemes.

5.2. Typical numerical results of temporary-plugging refracturing

Figs. 10 and 11 show the fracture morphology, injection pressure and fracture area of three typical cases of temporary-plugging refracturing.

When there is no temporary plugging, a planar fracture with a large area is mainly formed in the second cluster (Fig. 10a). The breakdown pressure is 54.08 MPa, and the extension pressure fluctuates from 45.1 to 48.9 MPa (Fig. 11a). During refracturing, only the fracture area of the second cluster increases rapidly, and the fracture area of the other two clusters stops increasing in the initial stage (less than 80 s). In the end, the fracture areas from the first to the third cluster are 142.41, 3020.05, and 237.60 m², respectively (Fig. 11a).

When the number of temporary plugging is 1, a planar fracture is effectively formed in the second cluster before the temporary plugging (600 s). After temporary plugging, the fracture in the second cluster stops propagation and its fracture area does not increase, and the injection pressure remains constant at 47.35 MPa. At this point, the fracture in the third cluster, with large rotated propagation near the wellbore due to the stress shadow effect, begins to effectively extend (Fig. 11b). There is also a slight increase

in the fracture area of the first cluster, from 142.33 to 172.09 m² (from 600 to 639 s) before the growth is stopped. This is because the fracturing fluid is forced to divert to the first and third clusters after the second cluster is plugged suddenly. During the temporary plugging, the injection pressure of the third cluster is increased sharply from 47.28 to 54.42 MPa, and the pressure difference before and after the temporary plugging is up to 7.14 MPa, and then the injection pressure is suddenly dropped to 46.67 MPa after the fracture in the third cluster extends (Fig. 11b). After fracturing, the fracture areas from the first cluster to the third cluster are 172.09, 2105.38, and 1948.56 m², respectively. The conclusion is that the change of injection pressure illustrates the temporary plugging effect, which indicates that the change in injection pressure can be used to describe and evaluate the temporary plugging in the field.

When the number of temporary plugging is 2, fractures effectively propagate from the second, the third, and the first cluster at 0, 400, and 800 s, respectively. A planar fracture is created in the second cluster, and fractures in the third and the first clusters are both curved and propagate outwards (Fig. 10c). As can be seen from Fig. 11c, the injection pressures before and after the first temporary plugging (at 400 s) are 45.74 and 53.87 MPa, an increase of 8.13 MPa. Similarly, we find that the injection pressure is increased

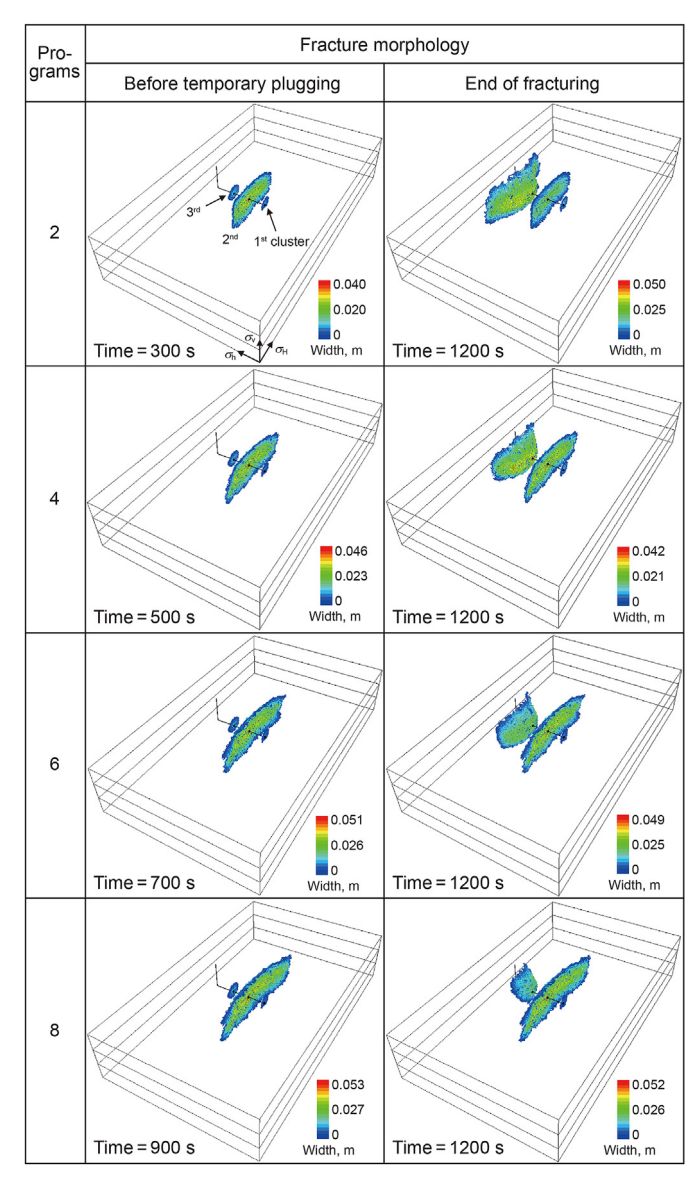


Fig. 13. Fracture morphologies with different temporary plugging timing when the number of temporary plugging is 1.

by 8.74 MPa during the second temporary plugging. After the first temporary plugging, the fracture area of the second cluster does not increase, and the fracture area of the first cluster increases slightly from 142.33 to 180.29 m² (400–437 s), and then stops propagation. The fracture area of the third cluster increases rapidly from 235.83 to 519.30 m² in the same period, and correspondingly the fracture in the third cluster becomes the dominant fracture. After the second temporary plugging, the fracture in the third cluster stops extending, and the fracture propagates from the first cluster. After fracturing, the fracture areas from the first cluster to the third cluster are 1272.33, 1751.07, and 1565.13 m², respectively.

5.3. Impact of essential factors of temporary-plugging refracturing

5.3.1. The number of temporary plugging

Fig. 12 shows the number of effective clusters, the normalized standard deviation of fracture area, and the total fracture area of different schemes. We find that applying temporary plugging diverters, especially with appropriate multiple temporary plugging,

can significantly increase the number of effective fractures, such as schemes 9, 10, 13, and 14 (Fig. 12a). The average normalized standard deviations for the cases with temporary plugging of 0, 1, and 2 are 0.39, 0.22, and 0.07, respectively, a decrease of 43.60% and 68.18%. The average total fracture areas of these three cases are 3400.07, 4065.22, and 4478.54 m², respectively, an increase of 19.56% and 10.17%. It shows that with increasing number of temporary plugging, the normalized standard deviation decreases sharply, and the total fracture area increases, indicating that multiple temporary plugging enhances the uniformity of multi-fracture propagation and improves the stimulation effect. Therefore, it is recommended to use multiple temporary plugging to obtain the optimal fracturing effect in the field.

5.3.2. Temporary plugging timing

Figs. 13 and 14 show fracture morphologies with different numbers of temporary plugging, 1 and 2, respectively. When the number of temporary plugging is 1, there are two effective clusters, as shown in Fig. 12a. With the temporary plugging timing increasing from 300 to 900 s, the dominant fracture of the second cluster propagates more fully, and the fracture area increases from 1483.10 to 2558.09 m² (Fig. 13). However, the fracture area of the other dominant fracture (the third cluster) is reduced by 54.96%. In addition, the normalized standard deviation of the fracture area decreases first and then increases as the temporary plugging timing increases (Fig. 12b), while the total fracture area increases first and then decreases. Therefore, for temporary-plugging refracturing with one temporary plugging, there is an optimal timing for temporary plugging to maximize the propagation uniformity of multicluster fractures and achieve the best fracturing results. In the case study, the fracturing effect is the best when the temporary plugging timing is 400 s, which is 1/3 of the total fracturing time. Obviously, the optimal temporary plugging timing is not 1/2 of the total fracturing time, which is related to the rapid growth of fracture area in the early stage and the slow growth in the later stage shown in

When the number of temporary plugging is 2, fracture morphologies vary significantly under different plugging timing, and an unreasonable setting of the temporary plugging timing (e.g., scheme 18) can result in a stimulation effect lower than that with just one temporary plugging (Fig. 14). Therefore, optimizing the temporary plugging timing for temporary-plugging refracturing is especially important. From Fig. 12, we can see that the total fracture area of scheme 10 is the largest with temporary plugging timing of 300 and 700 s, and the total fracture area of scheme 13 is the largest with temporary plugging timing of 400 and 700 s, and the normalized standard deviation is very small, indicating that the fracturing effect is the best. Therefore, with the temporary plugging number of 2, the optimal first temporary plugging timing is 1/4 to 1/3 of the total fracturing time, and the optimal second temporary plugging timing is 3/5 of the total fracturing time.

6. Analysis of field case of temporary-plugging refracturing

Fig. 15 shows the operating pressure curves for the pilot test of temporary-plugging refracturing of well P3. There are two applications of temporary plugging diverters. The major injection rate is 3 m³/min and the total fracturing time is 7622 s. The first temporary plugging timing is 1324–1710 s, which is about 1/5 of the total fracturing time, and the second temporary plugging timing is 4278–5050 s, about 3/5 to 2/3 of the total fracturing time.

The initial breakdown pressure is 50.28 MPa (state A) from the field injection pressure data, as shown in Fig. 15. Subsequently, the injection pressure drops rapidly (state B, at 1324 s), and then 100 kg temporary plugging diverters is placed, and the propagation of

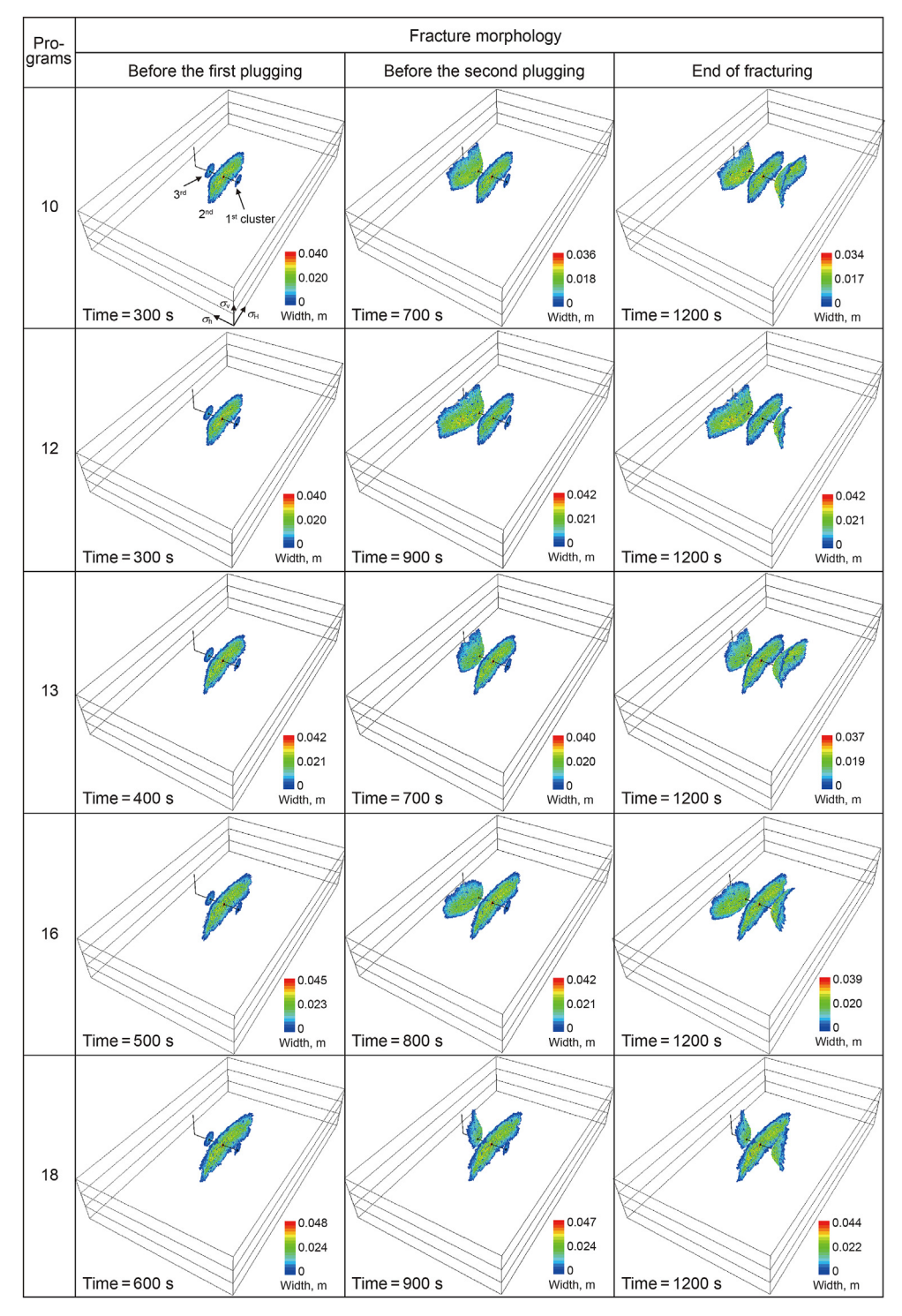


Fig. 14. Fracture morphologies with different temporary plugging timing when the number of temporary plugging is 2.

hydraulic fractures is limited. The reason is that the temporary plugging diverter is used too early. This results in the creation of small fractures that can be easily plugged by temporary plugging diverters, causing injection pressure to rise suddenly by 3.87 MPa from state B to state C. The injection pressure is then reduced by 5.44 MPa from state C to state D possibly due to the re-opening of fractures during the temporary plugging process. With more temporary plugging diverters, fractures are completely plugged and the injection pressure increases again by 5.88 MPa from state D to state

E. Therefore, it is concluded that the injection pressure is increased by 5.88 MPa during the first temporary plugging process. Then injection pressure drops by 5.04 MPa from state E to state F due to the generation of new fractures from other clusters.

After that, with the injection of proppant-carrying fluid, the injection pressure rises again from state F to state G. During the fracturing process from state G to state H, the injection pressure shows a steady downward trend with a reduction of 2.44 MPa, indicating that the fractures propagate smoothly. When placing

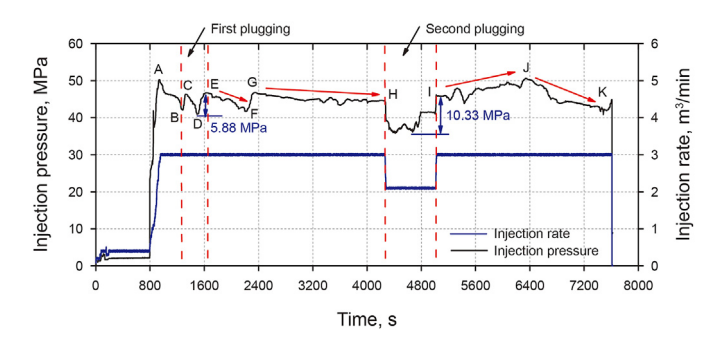


Fig. 15. Field operation curves of temporary-plugging refracturing of well P3.

200 kg temporary plugging diverter at state H, we find that the injection pressure fluctuates in a small range and the response of injection pressure change is relatively slow between state H and state I, which demonstrates that the process of temporary plugging is restricted and limited. The reason may be that between the first temporary plugging and the second one (1710–4278 s), large fractures are formed due to the excessive propagation of the dominant fractures, which makes the second temporary plugging difficult. The temporary plugging is achieved after a long period of temporary plugging, and the injection pressure rises (state I). During the second temporary plugging, the injection pressure increment is 10.33 MPa.

After the second temporary plugging from state I to state J, the injection pressure fluctuates frequently and shows an upward trend, indicating that the propagation of fractures is resisted, which may be related to the sand plugging. Injection pressure begins to drop overall after 6344 s (state J to state K), indicating normal propagation of fractures.

Compared with the above analyses and the results of Fig. 11c, we find that the errors in breakdown pressure, injection pressure increment of the first temporary plugging, and injection pressure increment of the second temporary plugging between the simulation results and field results are 7.56%, 38.26%, and 15.39%, respectively. These errors are considered to be within a reasonable range due to the challenges in fully considering the complex geological conditions and complex field operations in numerical simulation, which suggests the reliability of our numerical simulation. In addition, the response characteristics of injection pressure can be used to qualitatively evaluate the temporary plugging process. Too early temporary plugging can lead to rapid response of injection pressure because fractures have not fully propagated, but too late temporary plugging may cause the failure of temporary plugging because fractures have propagated excessively. These conclusions are also consistent with the aforementioned results from numerical simulations.

7. Conclusions

- (1) For conventional refracturing, high injection rate is beneficial to improve the balanced propagation of multi-cluster fractures and obtain the maximum total fracture area. However, the contribution of excessively high injection rate to the increase of stimulation effect is limited. Besides, increasing the cluster spacing can reduce the preferential propagation of dominant fractures, but the total fracture area first rises and then decreases. We find that an optimal cluster spacing (10 m) maximizes the total fracture area to 4409.85 m².
- (2) For temporary-plugging refracturing, multiple temporary plugging can improve the propagation uniformity of multicluster fractures and achieve the optimal stimulation effect.

- It is essential to optimize the number and timing of temporary plugging. Specifically, when the number of temporary plugging is only one, the optimal temporary plugging timing is 1/3 of the total fracturing time. When the number of temporary plugging is two, the optimal timing for the first temporary plugging is 1/4 to 1/3 of the total fracturing time, and for the second temporary plugging is 3/5 of the total fracturing time.
- (3) Field case analyses and numerical simulation results show that temporary plugging results in a significant increase in injection pressure, up to 5.88–10.33 MPa. This indicates that the process of temporary plugging during refracturing can be well identified and evaluated according to the response characteristics of injection pressure.

Declaration of competing interest

The authors declare that they have no known competing financial interests or personal relationships that could have appeared to influence the work reported in this paper.

Acknowledgments

This research is funded by the National Natural Science Foundation of China (41772286, 42077247), the Fundamental Research Funds for the Central Universities, and Open Research Fund of State Key Laboratory of Geomechanics and Geotechnical Engineering, Institute of Rock and Soil Mechanics, Chinese Academy of Sciences (Z020009). We also sincerely appreciate the useful discussion and guidance with Dr. Branko Damjanac on the discrete lattice method in hydraulic fracturing simulation.

References

Bakhshi, E., Golsanami, N., Chen, L., 2021. Numerical modeling and lattice method for characterizing hydraulic fracture propagation: a review of the numerical, experimental, and field studies. Arch. Comput. Methods Eng. 28, 3329–3360. https://doi.org/10.1007/s11831-020-09501-6.

Bakhshi, E., Rasouli, V., Ghorbani, A., et al., 2019. Lattice numerical simulations of lab-scale hydraulic fracture and natural interface interaction. Rock Mech. Rock Eng. 52, 1315–1337. https://doi.org/10.1007/s00603-018-1671-2.

Chen, M., Zhang, S., Zhou, T., et al., 2020. Optimization of in-stage diversion to promote uniform planar multifracture propagation: a numerical study. SPE J. 25, 3091–3110. https://doi.org/10.2118/201114-PA.

Cong, Z., Li, Y., Pan, Y., et al., 2022. Study on CO₂ foam fracturing model and fracture propagation simulation. Energy 238, 121778. https://doi.org/10.1016/j.energy.2021.121778.

Damjanac, B., Detournay, C., Cundall, P., et al., 2011. Xsite-description of Formulation. ITASCA Consulting Group., Inc.

Damjanac, B., Detournay, C., Cundall, P.A., 2016. Application of particle and lattice codes to simulation of hydraulic fracturing. Comput. Times Part Mech 3, 249–261. https://doi.org/10.1007/s40571-015-0085-0.

Feng, Y., Jones, J.F., Gray, K.E., 2016. A review on fracture-initiation and -propagation

Feng, Y., Jones, J.F., Gray, K.E., 2016. A review on fracture-initiation and -propagation pressures for lost circulation and wellbore strengthening. SPE Drill. Complet. 31, 134–144. https://doi.org/10.2118/181747-PA.

Feng, Y., Li, X., Gray, K.E., 2017. Development of a 3D numerical model for quantifying fluid-driven interface debonding of an injector well. Int. J. Greenh. Gas Control 62, 76–90. https://doi.org/10.1016/j.ijggc.2017.04.008.

Guo, J., Tao, L., Zeng, F., 2019. Optimization of refracturing timing for horizontal wells in tight oil reservoirs: a case study of Cretaceous Qingshankou formation, Songliao basin, NE China. Petrol. Explor. Dev. 46, 153–162. https://doi.org/ 10.1016/51876-3804(19)30015-1.

Guo, Y., Wang, L., Chang, X., et al., 2020. Study on fracture morphological characteristics of refracturing for Longmaxi shale formation. Geofluids 1–13. https://doi.org/10.1155/2020/1628431, 2020.

Gutierrez Escobar, R., Mejia Sanchez, E.C., Roehl, D., Romanel, C., 2019. XFEM modeling of stress shadowing in multiple hydraulic fractures in multi-layered formations. J. Nat. Gas Sci. Eng. 70, 102950. https://doi.org/10.1016/i.jngse.2019.102950.

Huang, J., Yang, C., Xue, X., Datta-Gupta, A., 2016. Simulation of coupled fracture propagation and well performance under different refracturing designs in shale reservoirs. In: SPE Low Perm Symposium. Society of Petroleum Engineers. https://doi.org/10.2118/180238-MS.

- Huang, L., Liu, J., Zhang, F., et al., 2020. 3D lattice modeling of hydraulic fracture initiation and near-wellbore propagation for different perforation models. J. Petrol. Sci. Eng. 191, 107169. https://doi.org/10.1016/j.petrol.2020.107169.
- Ishida, T., Fujito, W., Yamashita, H., et al., 2019. Crack expansion and fracturing mode of hydraulic refracturing from acoustic emission monitoring in a smallscale field experiment. Rock Mech. Rock Eng. 52, 543–553. https://doi.org/ 10.1007/s00603-018-1697-5.
- Li, J., Dong, S., Hua, W., et al., 2020a. Numerical simulation of temporarily plugging staged fracturing (TPSF) based on cohesive zone method. Comput. Geotech. 121, 103453. https://doi.org/10.1016/j.compgeo.2020.103453.
- Li, M., Guo, P., Stolle, D.F.E., et al., 2020b. Modeling hydraulic fracture in heterogeneous rock materials using permeability-based hydraulic fracture model. Undergr. Space 5, 167–183. https://doi.org/10.1016/j.undsp.2018.12.005.
- Li, M., Zhang, F., Zhuang, L., et al., 2020c. Micromechanical analysis of hydraulic fracturing in the toughness-dominated regime: implications to supercritical carbon dioxide fracturing. Comput. Geosci. 24, 1815–1831. https://doi.org/ 10.1007/s10596-019-09925-5
- Li, W., Zhao, H., Pu, H., et al., 2019. Study on the mechanisms of refracturing technology featuring temporary plug for fracturing fluid diversion in tight sandstone reservoirs. Energy Sci. Eng. 7, 88–97. https://doi.org/10.1002/ese3.259.
- Li, X., Wang, J., Elsworth, D., 2017. Stress redistribution and fracture propagation during restimulation of gas shale reservoirs. J. Petrol. Sci. Eng. 154, 150–160. https://doi.org/10.1016/j.petrol.2017.04.027.
- Liu, C., Dong, P., Zhu, B., Shi, Y., 2018. Stress shadow on the southwest portion of the Longmen Shan Fault impacted the 2008 Wenchuan earthquake rupture. J. Geophys. Res. Solid Earth 123, 9963–9981. https://doi.org/10.1029/ 2018B015633.
- Luo, L., Cheng, S., Lee, J., 2020. Characterization of refracture orientation in poorly propped fractured wells by pressure transient analysis: model, pitfall, and application. J. Nat. Gas Sci. Eng. 79, 103332. https://doi.org/10.1016/j.ingse.2020.103332.
- Manchanda, R., Sharma, M., Rafiee, M., Ribeiro, L., 2017. Overcoming the impact of reservoir depletion to achieve effective parent well re-fracturing. In: SPE/AAPG/ SEG Unconventional Resources Technology Conference. Unconventional Resources Technology Conference. https://doi.org/10.15530/urtec-2019-490.
- Mao, S., Zhang, Z., Chun, T., Wu, K., 2021. Field-scale numerical investigation of proppant transport among multicluster hydraulic fractures. SPE J. 26, 307–323. https://doi.org/10.2118/203834-PA.
- Marongiu-Porcu, M., Lee, D., Shan, D., Morales, A., 2016. Advanced modeling of interwell-fracturing interference: an Eagle Ford shale-oil study. SPE J. 21, 1567–1582. https://doi.org/10.2118/174902-PA.
- Mientka, M., Romberg, E., Scott, E., 2018. A novel approach to predicting improvements in perforation cluster treatment efficiency. In: SPE International Hydraulic Fracturing Technology Conference and Exhibition. Society of Petroleum Engineers. https://doi.org/10.2118/191467-18IHFT-MS.
- Nadimi, S., Forbes, B., Moore, J., McLennan, J.D., 2020. Effect of natural fractures on determining closure pressure. J. Pet. Explor. Prod. Technol. 10, 711–728. https:// doi.org/10.1007/s13202-019-00769-4.
- Ren, L., Zhao, J., Hu, Y., Xiong, X., 2010. Simulation on deviatoric fracture propagation path during refracturing process. In: International Conference on Computational and Information Sciences. IEEE.
- Rezaei, A., Bornia, G., Rafiee, M., et al., 2018. Analysis of refracturing in horizontal wells: insights from the poroelastic displacement discontinuity method. Int. J. Numer. Anal. Methods GeoMech. 42, 1306–1327. https://doi.org/10.1002/nag.2792.
- Roussel, N.P., Sharma, M.M., 2010. Quantifying transient effects in altered-stress refracturing of vertical wells. SPE J. 15, 770–782. https://doi.org/10.2118/119522-PA.
- Roussel, N.P., Sharma, M.M., 2012. Role of stress reorientation in the success of refracture treatments in tight gas sands. SPE Prod. Oper. 27, 346—355. https:// doi.org/10.2118/134491-PA.
- Roussel, N.P., Sharma, M.M., 2013. Selecting candidate wells for refracturing using production data. SPE Prod. Oper. 28, 36–45. https://doi.org/10.2118/146103-PA.
- Sangnimnuan, A., Li, J., Wu, K., 2018. Development of efficiently coupled fluid-flow/geomechanics model to predict stress evolution in unconventional reservoirs with complex-fracture geometry. SPE J. 23, 640–660. https://doi.org/10.2118/189452_PA
- Shah, M., Agarwal, J.R., Patel, D., et al., 2020. An assessment of chemical particulate technology as diverters for refracturing treatment. J. Nat. Gas Sci. Eng. 84, 103640. https://doi.org/10.1016/j.jngse.2020.103640.
- Shah, M., Shah, S., Sircar, A., 2017. A comprehensive overview on recent developments in refracturing technique for shale gas reservoirs. J. Nat. Gas Sci. Eng. 46, 350–364. https://doi.org/10.1016/j.jngse.2017.07.019.
- Taghichian, A., Zaman, M., Devegowda, D., 2014. Stress shadow size and aperture of hydraulic fractures in unconventional shales. J. Petrol. Sci. Eng. 124, 209–221. https://doi.org/10.1016/j.petrol.2014.09.034.
- Tan, P., Jin, Y., Pang, H., 2021. Hydraulic fracture vertical propagation behavior in transversely isotropic layered shale formation with transition zone using XFEM-based CZM method. Eng. Fract. Mech. 248, 107707. https://doi.org/ 10.1016/j.engfracmech.2021.107707.
- Tan, P., Pang, H., Zhang, R., et al., 2020. Experimental investigation into hydraulic fracture geometry and proppant migration characteristics for southeastern Sichuan deep shale reservoirs. J. Petrol. Sci. Eng. 184, 106517. https://doi.org/ 10.1016/j.petrol.2019.106517.

- Tang, J., Wu, K., Zuo, L., et al., 2019. Investigation of rupture and slip mechanisms of hydraulic fracture in multiple-layered formation. SPE J. 24, 2292–2307. https:// doi.org/10.2118/197054-PA.
- Wang, B., Zhou, F., Wang, D., et al., 2018. Numerical simulation on near-wellbore temporary plugging and diverting during refracturing using XFEM-Based CZM. J. Nat. Gas Sci. Eng. 55, 368–381. https://doi.org/10.1016/ i.ingse.2018.05.009.
- Wang, B., Zhou, F., Yang, C., et al., 2020. Experimental study on injection pressure response and fracture geometry during temporary plugging and diverting fracturing. SPE J. 25, 573–586. https://doi.org/10.2118/199893-PA.
- Wang, B., Zhou, F., Zou, Y., et al., 2019. Quantitative investigation of fracture interaction by evaluating fracture curvature during temporarily plugging staged fracturing. J. Petrol. Sci. Eng. 172, 559–571. https://doi.org/10.1016/j.petrol.2018.08.038.
- Wang, X., Luo, H., Zhang, F., 2022a. Parameter optimization for controlling the complexity of near-wellbore fractures for perforated fracturing from horizontal wells. Chin. J. Rock Mech. Eng. 41, 1223–1234. https://doi.org/10.13722/ j.cnki.jrme.2021.0868.
- Wang, X., Zhang, F., Tang, M., et al., 2022b. Effect of stress shadow caused by multistage fracturing from multiple well pads on fracture initiation and nearwellbore propagation from infill wells. SPE J. 27, 204–225. https://doi.org/ 10.2118/208577-PA.
- Wang, Y., Salehi, S., 2014. Refracture candidate selection using hybrid simulation with neural network and data analysis techniques. J. Petrol. Sci. Eng. 123, 138–146. https://doi.org/10.1016/j.petrol.2014.07.036.
- Wang, Z., Gao, D., Liu, J., 2016. Multi-objective sidetracking horizontal well trajectory optimization in cluster wells based on DS algorithm. J. Petrol. Sci. Eng. 147, 771–778. https://doi.org/10.1016/j.petrol.2016.09.046.
- Wu, J., Huang, H., Xu, E., et al., 2021. Numerical investigation on propagation behaviors of a three-dimensional fracture network coupled with microseismicity in fractured shale reservoirs. Energies 14, 8297. https://doi.org/10.3390/en14248297.
- Xie, J., Tang, J., Yong, R., et al., 2020. A 3-D hydraulic fracture propagation model applied for shale gas reservoirs with multiple bedding planes. Eng. Fract. Mech. 228, 106872. https://doi.org/10.1016/j.engfracmech.2020.106872.
- Yi, S., Manchanda, R., Sharma, M., Roussel, N., 2019. Preventing heel dominated fractures in horizontal well refracturing. In: SPE Hydraulic Fracturing Technology Conference and Exhibition. Society of Petroleum Engineers. https:// doi.org/10.2118/194341-MS.
- Yi, S., Sharma, M., 2016. A model for refracturing operations in horizontal wells employing diverting agents. In: SPE Asia Pacific Hydraulic Fracturing Conference. Society of Petroleum Engineers. https://doi.org/10.2118/181795-MS.
- Yi, S.S., Sharma, M.M., 2018. A new method to calculate slurry distribution among multiple fractures during fracturing and refracturing. J. Petrol. Sci. Eng. 170, 304–314. https://doi.org/10.1016/j.petrol.2018.06.048.
- Yue, Q., Liu, J., Zhang, L., Zhang, Q., 2018. The posting-buckling analysis and evaluations of limit drilling length for coiled tubing in the sidetrack horizontal well. J. Petrol. Sci. Eng. 164, 559–570. https://doi.org/10.1016/j.petrol.2018.01.061.
- Zhang, F., Damjanac, B., Maxwell, S., 2019a. Investigating hydraulic fracturing complexity in naturally fractured rock masses using fully coupled multiscale numerical modeling. Rock Mech. Rock Eng. 52, 5137—5160. https://doi.org/ 10.1007/s00603-019-01851-3.
- Zhang, F., Huang, L., Yang, L., et al., 2022. Numerical investigation on the effect of depletion-induced stress reorientation on infill well hydraulic fracture propagation. Pet Sci. 19 (1), 296–308. https://doi.org/10.1016/j.petsci.2021.09.014.
- Zhang, F., Mack, M., 2017. Integrating fully coupled geomechanical modeling with microsesmicity for the analysis of refracturing treatment. J. Nat. Gas Sci. Eng. 46, 16–25. https://doi.org/10.1016/j.jngse.2017.07.008.
- Zhang, F., Wang, X., Tang, M., et al., 2021a. Numerical investigation on hydraulic fracturing of extreme limited entry perforating in plug-and-perforation completion of shale oil reservoir in Changqing oilfield, China. Rock Mech. Rock Eng. 54, 2925–2941. https://doi.org/10.1007/s00603-021-02450-x.
- Zhang, F., Wu, J., Huang, H., et al., 2021b. Technological parameter optimization for improving the complexity of hydraulic fractures in deep shale reservoirs. Nat. Gas. Ind. 41, 125–135. https://doi.org/10.3787/j.issn.1000-0976.2021.01.011.
- Zhang, J., Li, Y., Pan, Y., et al., 2021c. Experiments and analysis on the influence of multiple closed cemented natural fractures on hydraulic fracture propagation in a tight sandstone reservoir. Eng. Geol. 281, 105981. https://doi.org/10.1016/ iengeeo.2020.105981.
- Zhang, J., Wang, G., He, K., Ye, C., 2019b. Practice and understanding of sidetracking horizontal drilling in old wells in Sulige Gas Field, NW China. Petrol. Explor. Dev. 46, 384–392. https://doi.org/10.1016/S1876-3804(19)60018-2.
- Zhang, L., Zhou, F., Mou, J., et al., 2020a. An integrated experimental method to investigate tool-less temporary-plugging multistage acid fracturing of horizontal well by using self-degradable diverters. SPE J. 25, 1204–1219. https:// doi.org/10.2118/199884-PA.
- Zhang, R., Hou, B., Tan, P., et al., 2020b. Hydraulic fracture propagation behavior and diversion characteristic in shale formation by temporary plugging fracturing. J. Petrol. Sci. Eng. 190, 107063. https://doi.org/10.1016/j.petrol.2020.107063.
- Zhang, T., Javadpour, F., Li, J., et al., 2021d. Pore-scale perspective of gas/water two-phase flow in shale. SPE J. 26, 828–846. https://doi.org/10.2118/205019-PA.
- Zhang, T., Javadpour, F., Yin, Y., Li, X., 2020c. Upscaling water flow in composite nanoporous shale matrix using lattice Boltzmann method. Water Resour. Res. 56. https://doi.org/10.1029/2019WR026007.
- Zhang, Y., Zhang, D., Wen, Q., et al., 2021e. Development and evaluation of a novel

- fracture diverting agent for high temperature reservoirs. J. Nat. Gas Sci. Eng. 93,
- 104074. https://doi.org/10.1016/j.jngse.2021.104074.
 Zhao, H., Wang, X., Liu, Z., 2019. Experimental investigation of hydraulic sand fracturing on fracture propagation under the influence of coal macrolithotypes in Hancheng block, China. J. Petrol. Sci. Eng. 175, 60–71. https://doi.org/10.1016/ j.petrol.2018.12.031.
- Zhao, H., Wang, X., Liu, Z., et al., 2018. Investigation on the hydraulic fracture propagation of multilayers-commingled fracturing in coal measures. J. Petrol.
- Sci. Eng. 167, 774–784. https://doi.org/10.1016/j.petrol.2018.04.028. Zhu, H., Deng, J., Jin, X., et al., 2015. Hydraulic fracture initiation and propagation from wellbore with oriented perforation. Rock Mech. Rock Eng. 48, 585–601. https://doi.org/10.1007/s00603-014-0608-7.
- Zou, Y., Ma, X., Zhang, S., 2020. Numerical modeling of fracture propagation during temporary-plugging fracturing. SPE J. 25, 1503–1522. https://doi.org/10.2118/